Journal of Solid State Chemistry **155,** 229–232 (2000)
doi:10.1006/jssc.2000.8938, available online at http://www.idealibrary.com on IDEAL®

A New High-Efficiency UV-Emitting X-Ray Phosphor, $BaHf_{1-x}Zr_x(PO_4)_2$

C. R. Miao and C. C. Torardi[1]

Central Research and Development, DuPont Company, Experimental Station, Wilmington, Delaware 19880-0356

DEDICATED TO PROFESSOR J. M. HONIG

Barium hafnium–zirconium phosphate $BaHf_{1-x}Zr_x(PO_4)_2$ ($x = 0$–0.2), having the monoclinic $KFe(SO_4)_2$ (Yavapaiite) structure, is a broad-band UV-emitting phosphor. At room temperature, it has an emission peak maximum at approximately 356 nm under 30 kV peak molybdenum X-ray excitation. Compositions derived from 99% pure hafnia and having nominal values of $x \sim 0.01$–0.05 demonstrate luminescence efficiencies that make $BaHf_{1-x}Zr_x(PO_4)_2$ 30% brighter than $CaWO_4$ Hi-Plus. This efficiency is equal to that of a commercial M'–$YTaO_4$ phosphor that emits at 330 nm. $BaHf_{1-x}Zr_x(PO_4)_2$ is, thus, a potentially attractive candidate for use in medical diagnostic imaging systems. The lower X-ray absorption of $BaHf_{1-x}Zr_x(PO_4)_2$, relative to that of UV-emitting M'–$YTaO_4$, suggests that the title phosphor may be suitable for two-sided mammography screen applications. The synthesis conditions, X-ray excited luminescence, and effects of Eu, Sn, and Ti doping are discussed. © 2000 Academic Press

Key Words: **barium hafnium phosphate; zirconium luminescence; X-ray phosphor; UV emission.**

INTRODUCTION

X-ray phosphors are solid-state inorganic materials used in medical X-ray imaging applications (1, 2). The purpose in using these phosphors is to reduce the exposure of the patient to X-rays while maintaining the structural features of the X-ray image. Phosphor "intensifying screens" absorb X-ray photons and convert each photon's energy into hundreds of visible or UV light photons that are then recorded by a detector, such as a piece of photographic film. Good X-ray phosphors must fulfill several challenging requirements (1–3): good X-ray absorption in the diagnostic medical energy range (15–100 keV), high luminescence efficiency, emission in the green to near-UV region, proper crystallite size and shape, air and water stability, and easy large-scale production.

Replacement of visible-light-emitting phosphors with UV-emitting M'–$YTaO_4$ was found to significantly improve radiographic image sharpness (4, 5). There are two reasons for the improvement in image quality. First, the UV light is more highly attenuated within the intensifying screen and the image emanating from the screen (i.e., the cone of emission) is sharper than that of comparable visible-light-emitting screens. Second, "print-through" is virtually eliminated because the UV light emitted from the intensifying screen is more efficiently absorbed by the silver halide emulsion, and, in addition, any remaining UV light that transmits through the emulsion is attenuated by the film base (2).

These advantages over visible-light-emitting phosphors have focused current research and development efforts on finding other UV-emitting X-ray phosphors (i.e., those with emission less than 400 nm). Attention has been given to hafnium-oxide-based phosphors because HfO_2 and hafnate compounds have good X-ray absorption and relatively large band gaps. For example, blue- and UV-emitting hafnium X-ray phosphors, $Hf_{1-x}Ti_xO_2$ (6) and $Hf_{1-x}Zr_xGeO_4$ (7), respectively, have been developed in recent years by the Eastman Kodak Company.

In this paper, we discuss the synthesis, structure, chemistry, and luminescence of an efficient UV-emitting X-ray phosphor $BaHf_{1-x}Zr_x(PO_4)_2$ ($x = 0$–0.2). The optimum chemical composition region, having nominal $x \sim 0.01$–0.05, results in ultraviolet, broad-band X-ray-excited luminescence, peaking at $\sim$356 nm, with intensity comparable to that of UV-emitting M'–$YTaO_4$, a very successful commercial phosphor (4).

EXPERIMENTAL

Synthesis

$BaHf_{1-x}Zr_x(PO_4)_2$ ($x = 0.0$–0.2) was prepared by grinding and reacting stoichiometric quantities of $BaCO_3$, HfO_2 (preferably using cheaper, 99% purity hafnia), ZrO_2, and $NH_4H_2PO_4$ in an alumina crucible at 1100°C for about 12 hours in air. The amount of Zr present in 99% pure HfO_2 was ignored in calculating the quantity of ZrO_2 required for any x value. For example, a preparation designed to have $x = 0$ used 99% pure HfO_2 and no ZrO_2. A typical synthesis for the optimal composition, $BaHf_{0.97}Zr_{0.03}(PO_4)_2$, consisted of mixing in an agate mortar 3.0000 g of $BaCO_3$ (Fisher Certified A.C.S.), 3.1041 g of HfO_2 (Johnson

[1] To whom correspondence should be addressed. Fax: (302)695-1664. E-mail: charlie.c.torardi@usa.dupont.com.

0022-4596/00 $35.00

Matthey 99%), 0.0562 g of ZrO_2 (Johnson Matthey 99 + %), and 3.4958 g of $NH_4H_2PO_4$ (Baker 99.95%), and then heating this reaction mixture in an alumina crucible in air, ramping up to 1100°C in 3 hours, and soaking for 12 hours, followed by furnace cooling. Higher purity, optical-grade starting materials were also used and gave comparable results; HfO_2 (Johnson Matthey 99.9%), ZrO_2 (Johnson Matthey 99.99%), and $NH_4H_2PO_4$ (Johnson Matthey 99.998%).

X-ray powder diffraction patterns of the products with $x < 0.2$ showed the lines of $BaHf(PO_4)_2$ (JCPDS-ICDD card no. 33-150) and only very small amounts of HfO_2 (JCPDS-ICDD card no. 34-104) as an impurity. The product with $x = 0.2$ displayed additional low-level impurities due to HfP_2O_7/ZrP_2O_7 and some other unidentified peaks. Reactions designed to make the $x = 0.6$ and 1.0 materials at 1100°C gave mixed-phase products with significant amounts of impurities. However, the phosphor properties (e.g., density and luminescence efficiency) of such compositions were outside our range of interest, and, therefore, not studied further.

Reactants used in activator doping studies were TiO_2 (Aldrich 99.999%), SnO_2 (Johnson Matthey 99.9%), and Eu_2O_3 (Johnson Matthey 99.99%). Flux reaction experiments employed LiCl (Baker A.C.S. reagent grade) and Li_2SO_4 (Lithco/FMC 99% minimun). The doping and flux reactions are discussed in detail below.

The particle size, crystallite size, and morphology were examined using scanning electron microscopy.

X-Ray Luminescence Measurements

For measurements of X-ray-stimulated luminescence properties, the powders were first mixed with a polymeric binder and coated on a sheet of base material. This technique for making a phosphor "screen" is similar to that used in commercial production, and permits the preparation of a screen with a uniform thickness of uniformly dense material. A cardboard base material and carboxylated methyl methacrylate acrylic binder were chosen to avoid interference with the X-ray luminescence measurements.

The X-ray luminescence of the samples was examined under ambient conditions using a molybdenum X-ray source operating at 30 kV (peak voltage) and 10 mA. The sample was exposed to polychromatic X-radiation, and two detectors were used to measure the luminescence properties (2). The first detection system consisted of a Hamamatsu R928 photomultiplier and a picoammeter, and was used to measure the total intensity of light coming from the sample, or the overall X-ray-to-light conversion efficiency. The second detection system used a SPEX 500M spectrometer, in which the light from the sample passes through a 0.5-meter monochromator before entering a Hamamatsu R928 photomultiplier. Using this detection system, a characteristic spectrum of the luminescence of the sample could be obtained by scanning through the range of detectable wavelengths allowed by the monochromator, and measuring the intensity of light at each interval. The Hamamatsu photomultipliers were selected because of their relatively flat response in the region 300–600 nm.

RESULTS AND DISCUSSION

Structure

The crystal structure of $BaHf(PO_4)_2$ is essentially identical to those of $BaZr(PO_4)_2$ and low-temperature $BaTi(PO_4)_2$, all having the $KFe(SO_4)_2$ Yavapaiite structure (8). The hafnium compound is monoclinic, $C2/m$ with $a = 8.550$ Å, $b = 5.296$ Å, $c = 7.883$ Å, and $\beta = 93.13°$ (JCPDS-ICDD card no. 33-150). By analogy with the reported single-crystal structure of $KFe(SO_4)_2$ (8), the structure of $BaHf(PO_4)_2$ contains hafnium in octahedral coordination with oxygen atoms from six separate phosphate groups (Fig. 1). The hafnium phosphate octahedra are interconnected in two dimensions to form layers (Fig. 1). Barium ions, located between the layers, are 10-coordinated to phosphate oxygen atoms.

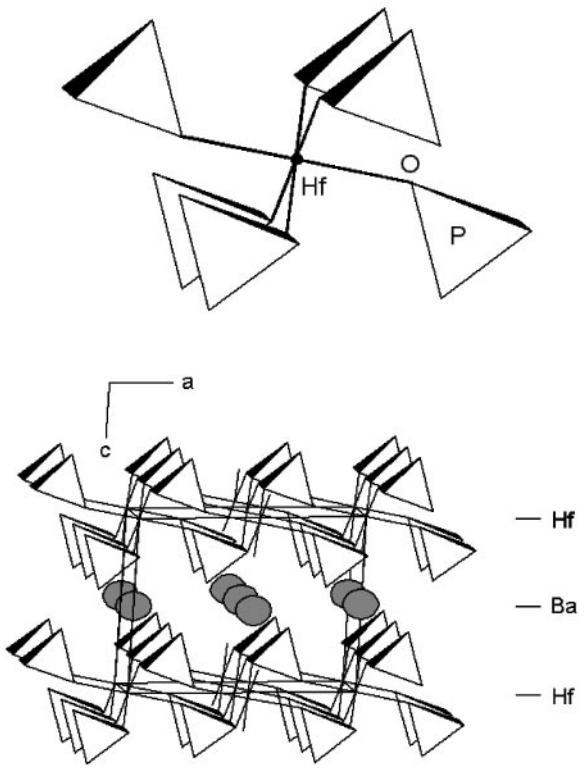

FIG. 1. Top: octahedral arrangement of six phosphate groups bonded to one Hf ion in the monoclinic unit cell of $BaHf(PO_4)_2$. Bottom: hafnium phosphate octahedra interconnected in two dimensions forming layers separated by Ba ions.

Synthesis and Characterization

The synthesis of $BaHf_{1-x}Zr_x(PO_4)_2$ phosphor was easily and reproducibly performed by conventional solid-state reaction of $BaCO_3$, HfO_2, ZrO_2, and $NH_4H_2PO_4$. The 99% grade hafnia, which typically contains $\sim$1–2 weight percent zirconium (metals basis), was used because of its relatively low cost (obviously, a major consideration for commercial use). These levels of zirconium in hafnia translate into a Zr/Hf mole ratio range of $\sim$0.02–0.04. In our studies, the amount of Zr in 99% pure HfO_2 was ignored in calculating the quantities of ZrO_2 required for any x value, and the reported x values are, therefore, considered only nominal values. The actual zirconium content of the phosphor is higher.

The optimum reaction temperature is 1100°C. A higher level of phase impurity, mainly HfO_2, was observed for the products made at 1000°C, whereas firing at 1200°C resulted in an almost 30% loss in luminescence efficiency. The reason for this decrease in efficiency is not understood. All of the higher temperature preparations contained a very small amount of unreacted HfO_2, the amount decreasing with increasing reaction temperature. The HfO_2 was observed even after the product was ground and reheated at 1100°C. However, this was not of major concern in the luminescence study because bulk, 99% grade HfO_2 is a very weak X-ray phosphor, exhibiting $\sim$2% the efficiency of $BaHf_{0.97}Zr_{0.03}(PO_4)_2$ and M'–$YTaO_4$.

SEM images of the 1100°C reaction products, which gave the highest luminescence efficiencies, showed submicron to 10-μm irregularly shaped crystallites that were fused into 5–100-μm agglomerates. Simple hand-grinding of the phosphor under acetone in a mortar effectively separated the crystallites (Fig. 2).

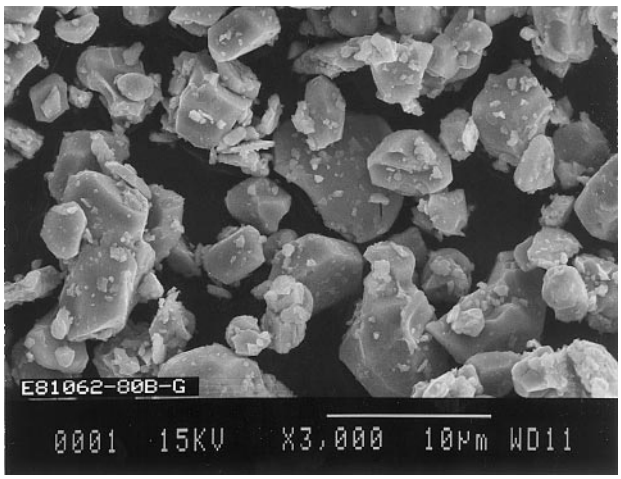

FIG. 2. Scanning electron micrograph of $BaHf_{1-x}Zr_x(PO_4)_2$ (with nominal $x = 0.03$) synthesized at 1100°C.

To better control the morphology of the phosphor, we carried out flux reactions using LiCl and Li_2SO_4. We have recently discussed the benefits of using fluxes in the synthesis of phosphor materials (2, 9–11). Typically, large quantities of flux ($\sim$25–100 wt%) are mixed with the reactants. Such high levels of flux are not feasible in making $BaHf_{1-x}Zr_x(PO_4)_2$ because LiCl and Li_2SO_4 stabilize the formation of $Ba_5Cl(PO_4)_3$ and $BaSO_4$, respectively. However, we found that by decreasing the amount of these fluxes to a Li/Hf mole ratio of $\sim$0.2, more crystalline and phase-pure products could be made. Scanning electron micrographs showed a uniform particle size distribution of $\sim$10–60 μm, which, unfortunately, is too large for use in a commercial phosphor screen. Also, all of the flux-derived products displayed a 25–40% decrease in luminescence efficiency. Because of this detrimental effect on efficiency, the flux study was discontinued.

Titanium- and tin-doped samples were made in the same manner as the zirconium-doped specimens. The compositions were $BaHf_{1-y}Ti_y(PO_4)_2$, with $y = 0.01$, 0.03, and 0.05 and nominal $x = 0.0$, and $BaHf_{1-y}Sn_y(PO_4)_2$, with $y = 0.005$, 0.010, and 0.030 and nominal $x = 0.0$. $Ba_{1-y}Eu_yHf(PO_4)_2$ ($y = 0.005$, 0.010, and 0.030 with nominal $x = 0.0$) samples were synthesized in two steps: first, firing in air, as usual, at 1100°C for 12 hours, and then heating in flowing 2% H_2 in argon at 900°C. XPD patterns showed $BaHf(PO_4)_2$ plus a small amount of HfO_2.

X-Ray-Excited Luminescence

The X-ray-excited emission spectra of $BaHf_{1-x}Zr_x(PO_4)_2$ with nominal x values of 0.0–0.2 are shown in Fig. 3. All exhibit broad-band emission with a peak in the ultraviolet at approximately 356 nm, a bandwidth of 100 nm, and a tail extending into the blue region (> 400 nm). The emission characteristics are similar to those of Zr-doped $HfGeO_4$ (7) that was also derived from a lower purity grade of HfO_2.

For $BaHf_{1-x}Zr_x(PO_4)_2$ with $x = 0.0$ (Fig. 3), a significant intensity of emission is observed due to the small amount of zirconium in the starting 99% purity hafnia. This means that the nominal composition of $x = 0.0$ actually has $x \sim 0.02$–0.04, as discussed above. Note, therefore, that the emission intensity at any nominal value of x reported in this paper for $BaHf_{1-x}Zr_x(PO_4)_2$ will vary with the zirconium content of the HfO_2 starting material. For example, a comparison of phosphors having nominal $x = 0.03$ made from 99% pure HfO_2 and from high-purity HfO_2 showed the latter to have lower emission intensity. Other impurities, such as iron, in the hafnium oxide may also affect the intensity.

The shoulder at $\sim$410 nm on the emission peak for the $x = 0.20$ sample (Fig. 3) is attributed to the impurities seen

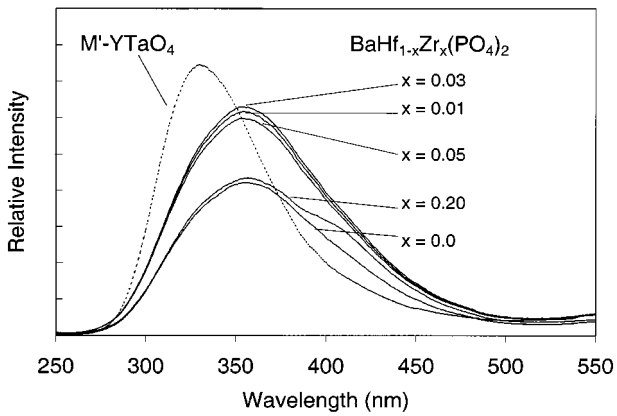

FIG. 3. X-ray-excited UV emission spectra of $BaHf_{1-x}Zr_x(PO_4)_2$ having nominal x values of 0.0–0.2 (see text), and a comparison with the emission spectrum of commercial M'–$YTaO_4$ phosphor.

in the XPD pattern. Maximum efficiency was obtained at nominal $x \sim 0.01$–0.05. These compositions demonstrate luminescence efficiencies that make $BaHf_{1-x}Zr_x(PO_4)_2$ 30% brighter than standard $CaWO_4$ Hi-Plus. The luminescence efficiency is equal to that of commercial M'–$YTaO_4$ phosphor (1, 2, 4) that emits at 330 nm. Emission spectra for M'–$YTaO_4$ and $BaHf_{0.97}Zr_{0.03}(PO_4)_2$ are compared in Fig. 3. Perhaps the only commercial disadvantage of $BaHf_{1-x}Zr_x(PO_4)_2$ is the lower X-ray absorption relative to that of M'–$YTaO_4$ (it has only 62% of the density of $YTaO_4$, 4.71 vs 7.58 g/cm^3). Nonetheless, a UV-emitting phosphor that is as bright as M'–$YTaO_4$ could be of interest to the X-ray phosphor industry, and it may be suitable for two-sided mammography screen applications (12).

Doping studies were performed with the intent of tuning the emission toward the blue region. The activators selected for this purpose were Eu^{2+}, Sn^{4+}, and Ti^{4+}. No emission from these ions, and no shift in the position of the zirconium emission peak, was found at the dopant levels described above. A general effect was a steady decrease in the 356 nm emission intensity with increase of dopant level. In the case of europium, emission spectra were identical before and after firing in H_2/Ar, and, in addition to the UV peak, only very weak Eu^{3+} red emission was recorded between 580–630 nm.

Titanium was more effective in quenching the zirconium emission than was europium or tin. At concentration $y = 0.01$, the europium- and tin-doped materials had 35% of the emission intensity relative to $y = 0.0$. For titanium at $y = 0.01$, only very weak emission remained. The latter is consistent with the luminescence of the isostructural compounds $BaTi(PO_4)_2$ and $BaZr_{0.95}Ti_{0.05}(PO_4)_2$ (13). Under UV excitation at temperatures below 100 K, both compounds have yellow emission at $\sim$510 nm due to TiO_6 octahedra. In $BaHf_{1-y}Ti_y(PO_4)_2$, energy transfer most likely occurs from the host lattice, or via the zirconium activator, to the Ti^{4+} ions, which are at lower energy than zirconium. At room temperature, however, the titanium luminescence is thermally quenched.

ACKNOWLEDGMENT

We thank M. K. Crawford, S. L. Issler, W. Zegarski, and L. H. Brixner for discussions on phosphor materials, B. D. Jones for assistance with the X-ray excitation spectrometer, and C. M. Foris for X-ray powder diffraction data.

REFERENCES

1. L. H. Brixner, *Mater. Chem. Phys.* **16,** 253 (1987).
2. S. L. Issler and C. C. Torardi, *J. Alloys Compd.* **229,** 54 (1995).
3. R. C. Ropp, "Luminescence and the Solid State." Elsevier Science, Amsterdam, 1991.
4. L. H. Brixner and H.-y. Chen, *J. Electrochem. Soc.* **130,** 2435 (1983).
5. J. Beutel, D. J. Mickewich, S. L. Issler, and R. Shaw, *Phys. Med. Biol.* **38,** 1195 (1993).
6. P. S. Bryan, P. M. Lambert, C. M. Towers, and G. S. Jarrold, U.S. Patent 4,988,880, 1989.
7. P. M. Lambert, P. S. Bryan, G. S. Jarrold, and C. M. Towers, U.S. Patent 5,173,611, 1992.
8. E. J. Graeber and A. Rosenzweig, *Am. Mineral.* **56,** 1917 (1971).
9. D. B. Hedden, C. C. Torardi, and W. Zegarski, *J. Solid State Chem.* **118,** 419 (1995).
10. C. R. Miao and C. C. Torardi, *J. Solid State Chem.* **145,** 110 (1999).
11. C. R. Miao and C. C. Torardi, U.S. Patent 5,611,960, 1997.
12. J. Beutel, S. L. Issler, and D. J. Mickewich, U.S. Patent 5,367,172, 1994.
13. G. Blasse and G. J. Dirksen, *Chem. Phys. Lett.* **62,** 19 (1979).